Crystal structure of nicarbazin, $(C_{13}H_{10}N_4O_5)(C_6H_8N_2O)$

James A. Kaduk [1,2,a], A. Dosen [3] and Thomas N. Blanton [3]
[1]*Illinois Institute of Technology, 3101 S. Dearborn St., Chicago, IL 60616, USA*
[2]*North Central College, 131 S. Loomis St., Naperville, IL 60540, USA*
[3]*ICDD, 12 Campus Blvd., Newtown Square, PA, 19073-3273, USA*

(Received 23 January 2024; accepted 1 March 2024)

The crystal structure of nicarbazin has been solved and refined using synchrotron X-ray powder diffraction data and optimized using density functional theory techniques. Nicarbazin is a co-crystal of 4,4′-dinitrocarbanilide (DNC) and 2-hydroxy-4,6-dimethylpyrimidine (HDP) molecules. Nicarbazin crystallizes in space group *P-1* (#2) with $a = 6.90659(8)$, $b = 12.0794(4)$, $c = 13.5040(7)$ Å, $\alpha = 115.5709(11)$, $\beta = 102.3658(6)$, $\gamma = 91.9270(4)°$, $V = 982.466(5)$ Å^3, and $Z = 2$. The DNC and HDP molecules are linked by two strong N–H···O and N–H···N hydrogen bonds, and the HDP molecules are linked into centrosymmetric dimers by another N–H···O hydrogen bond. These strong hydrogen bonds link the molecules into layers parallel to the *ab*-plane and parallel stacking of both DNC and HDP molecules is prominent in the structure. The powder pattern has been submitted to ICDD for inclusion in the Powder Diffraction File™ (PDF®).

[doi:10.1017/S0885715624000125]

Keywords: nicarbazin, Carbigran®, crystal structure, Rietveld refinement, density functional theory

I. INTRODUCTION

Nicarbazin (sold under the brand names Carbigran®, Nicarb®, and many others) is an equimolar complex of 4,4′-dinitrocarbanilide and 2-hydroxy-4,6-dimethylpyrimidine. It is used as a coccidiostat for poultry by inhibiting the reproduction of coccidia parasites, particularly in chickens selected for human consumption. Nicarbazin also finds application as a contraceptive for Canada geese and pigeons. The systematic name (CAS Registry Number 330-95-0) is 1,3-bis(4-nitrophenyl)urea 4,6-dimethyl-1H-pyrimidin-2-one. A two-dimensional molecular diagram is shown in Figure 1.

Nicarbazin can be obtained by the reaction of 4,4′-dinitrocarbanilide (DNC) and 2-hydroxy-4,6-dimethylpyrimidine (HDP) in methanol (Rogers et al., 1983). Such complexes are prepared to enhance the solubility of DNC in water, but re-crystallization (to single crystals) proved impossible. We are unaware of any published X-ray powder diffraction data for nicarbazin.

This work was carried out as part of a project (Kaduk et al., 2014) to determine the crystal structures of large-volume commercial pharmaceuticals and include high-quality powder diffraction data for them in the Powder Diffraction File (Gates-Rector and Blanton, 2019).

II. EXPERIMENTAL

Nicarbazin was a commercial reagent, purchased from TargetMol (Batch #114902), and was used as-received. The white powder was packed into a 1.5 mm diameter Kapton capillary and rotated during the measurement at ~50 Hz. The powder pattern was measured at 295 K at beam line 11-BM (Antao et al., 2008; Lee et al., 2008; Wang et al., 2008) of the Advanced Photon Source at Argonne National Laboratory using a wavelength of 0.458208(2) Å from 0.5° to 50° 2θ with a step size of 0.001° and a counting time of 0.1 s/step. The high-resolution powder diffraction data were collected using 12 silicon crystal analyzers that allow for high angular resolution, high precision, and accurate peak positions. A mixture of silicon (NIST SRM 640c) and alumina (NIST SRM 676a) standards (ratio Al_2O_3:Si = 2:1 by weight)

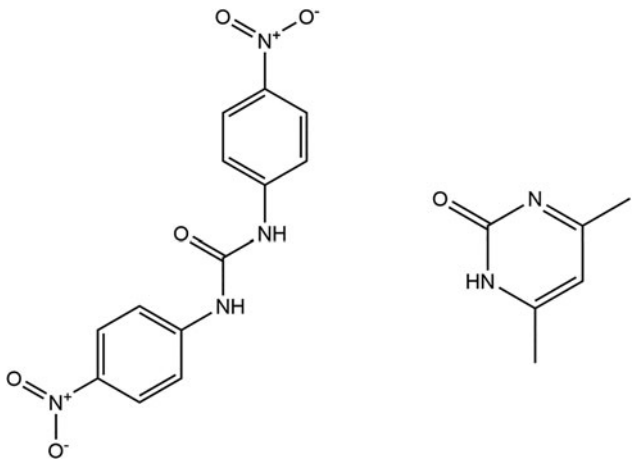

Figure 1. The 2D molecular structure of nicarbazin. The 4,4′-dinitrocarbanilide molecule is on the left, and 2-hydroxy-4,6-dimethylpyrimidine is on the right.

[a]Author to whom correspondence should be addressed. Electronic mail: kaduk@polycrystallography.com

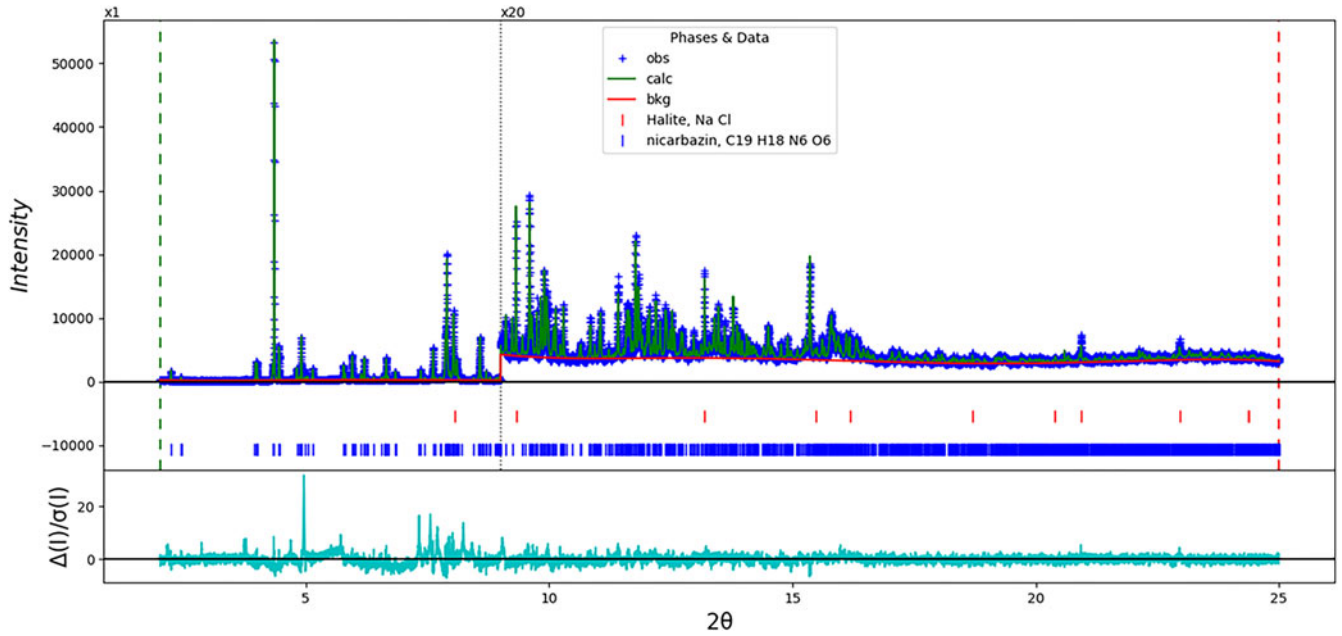

Figure 2. The Rietveld plot for the refinement of nicarbazin. The blue crosses represent the observed data points, and the green line is the calculated pattern. The red line is the background curve. The cyan curve is the normalized error plot. The vertical scale has been multiplied by a factor of 20× for $2\theta > 9.0°$.

was used to calibrate the instrument and refine the monochromatic wavelength used in the experiment.

The pattern was indexed using peaks of >1% relative intensity with JADE Pro 8.6 (MDI, 2022) on a high-quality primitive triclinic unit cell with $a = 6.90659$, $b = 12.0794$, $c = 13.5040$ Å, $\alpha = 115.5709$, $\beta = 102.3658$, $\gamma = 91.9270°$, $V = 982.466$ Å^3, and $Z = 2$. The suggested space group was *P-1*, which was confirmed by the successful solution and refinement of the structure. A reduced cell search in the Cambridge Structural Database (Groom et al., 2016) yielded one hit, but no related structures.

Structures of the constituent molecules were downloaded from PubChem (Kim et al., 2019) as Conformer3D_CID_1511764.sdf and Conformer3D_CID_9509.sdf. Conformer3D_CID_1511764.sdf was trimmed to remove substituents. They were converted to *.mol2 files using Mercury (Macrae et al., 2020), and to Fenske–Hall *Z*-matrices using Open Babel (O'Boyle et al., 2011). The structure was solved using FOX (Favre-Nicolin and Černý, 2002) using $\sin\theta/\lambda_{max} = 0.32$ Å^{-1}. Analysis of potential hydrogen bonding patterns indicated that N35 was protonated (N3···O33~2.4 Å), so H49 was added to N35 using Materials Studio (Dassault Systèmes, 2021).

Rietveld refinement was carried out using GSAS-II (Toby and Von Dreele, 2013). Only the 2.0–25.0° portion of the pattern was included in the refinement ($d_{min} = 1.058$ Å). Initial refinements indicated the presence of extra (unindexed) peaks. NaCl was identified as being present and was added to the refinement as a second phase. Its concentration refined to 0.6 wt.%. A few very weak additional peaks indicated the presence of at least one additional impurity phase. All non-H-bond distances and angles were subjected to restraints, based on a Mercury/Mogul Geometry Check (Bruno et al., 2004; Sykes et al., 2011). The Mogul average and standard deviation for each quantity were used as the restraint parameters. The restraints contributed 1.4% to the final χ^2. The hydrogen atoms were included in calculated positions, which were recalculated during the refinement using Materials Studio (Dassault Systèmes, 2021). The U_{iso} was grouped by chemical similarity. The U_{iso} for the H atoms was fixed at 1.3× the U_{iso} of the heavy atoms to which they are attached. A second-order

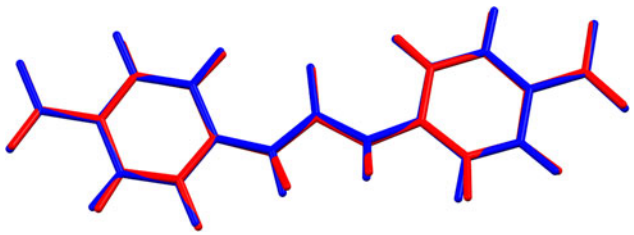

Figure 3. Comparison of the Rietveld-refined (red) and VASP-optimized (blue) structures of the 4,4′-dinitrocarbanilide (DNC) molecule in nicarbazin. The rms Cartesian displacement is 0.069 Å. Image generated using Mercury (Macrae et al., 2020).

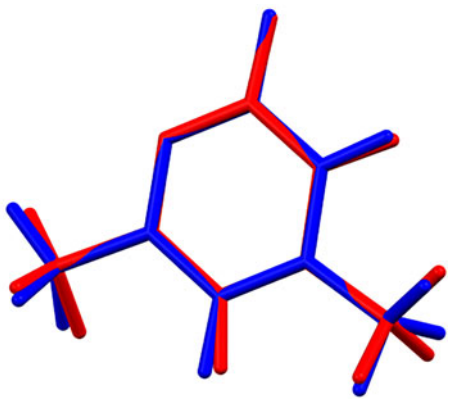

Figure 4. Comparison of the Rietveld-refined (red) and VASP-optimized (blue) structures of the 2-hydroxy-4,6-dimethylpyrimidine (HDP) molecule in nicarbazin. The rms Cartesian displacement is 0.026 Å. Image generated using Mercury (Macrae et al., 2020).

https://doi.org/10.1017/S0885715624000125 Published online by Cambridge University Press

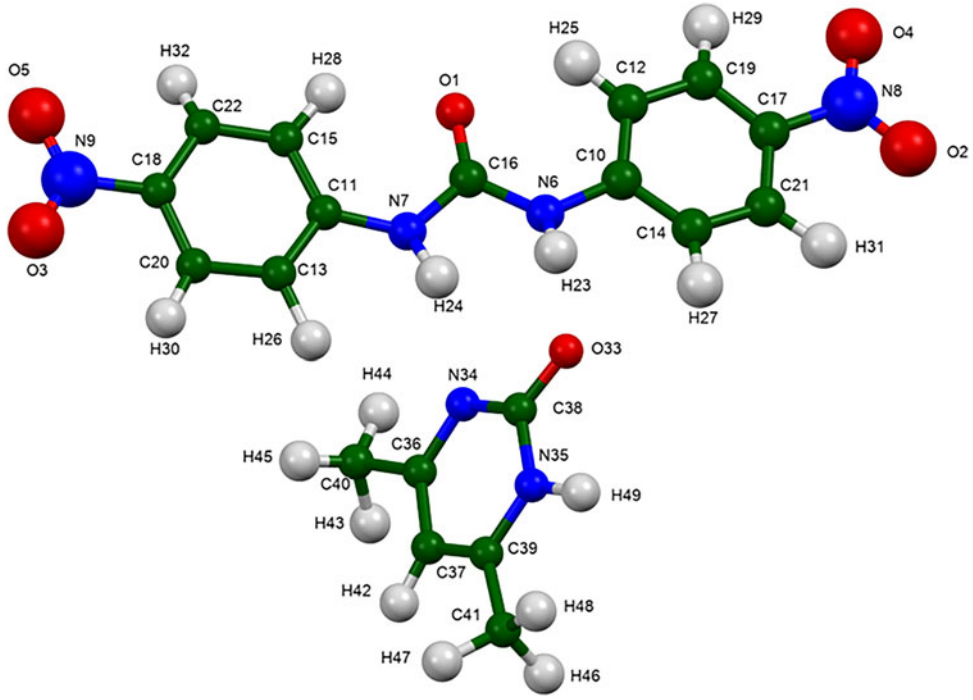

Figure 5. The asymmetric unit of nicarbazin, with the atom numbering. The atoms are represented by 50% probability spheroids. Image generated using Mercury (Macrae et al., 2020).

spherical harmonic model was included in the refinement. The refined texture index was 1.001(0). The peak profiles were described using the generalized microstrain model. The background was modeled using a six-term shifted Chebyshev polynomial, plus a peak at 5.86° 2θ to model the scattering from the Kapton capillary and any amorphous component.

The final refinement of 136 variables using 23,037 observations and 75 restraints yielded the residuals $Rwp = 0.0991$ and goodness of fit (GOF) = 1.90. The largest peak (0.32 Å from N7) and hole (1.62 Å from C20) in the difference Fourier map were 0.31(6) and −0.23(6) eÅ^{-3}, respectively. The largest errors in the difference plot (Figure 2) are attributed to impurity peaks.

The crystal structure of nicarbazin was optimized (fixed experimental cell) and population analysis was carried out using density functional theory techniques as implemented

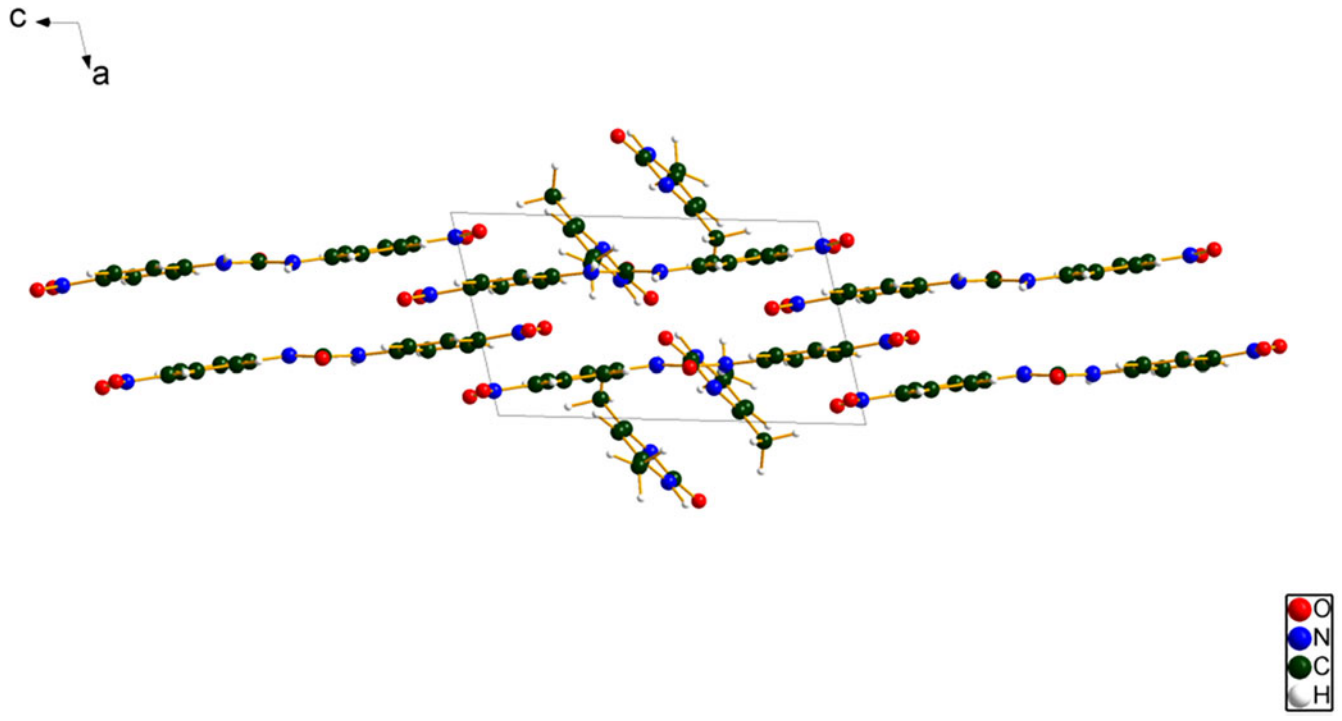

Figure 6. The crystal structure of nicarbazin, viewed down the *b*-axis. Image generated using Diamond (Crystal Impact, 2022).

https://doi.org/10.1017/S0885715624000125 Published online by Cambridge University Press

TABLE I. Hydrogen bonds (CRYSTAL17) in nicarbazin

H-bond	D–H, Å	H···A, Å	D···A, Å	D–H···A,◦	Overlap, *e*	*E*, kcal/mol
N35–H49···O33	1.037	1.773	2.774	179.2	0.077	6.4
N7–H24···N34	1.031	1.899	2.891	174.6	0.064	
N6–H23···O33	1.025	1.945	2.942	170.8	0.059	5.6
C37–H42···O2	1.080	2.420	3.253	128.1	0.019	
C40–H45···O4	1.092	2.411	3.397	149.0	0.017	
C40–H43···O3	1.096	2.612	3.253	123.9	0.015	
C12–H25···O1	1.079	2.170[a]	2.862	120.4	0.023	
C19–H29···O4	1.082	2.394[a]	2.731	95.5	0.016	
C21–H31···O5	1.081	2.468	3.218	117.1	0.013	
C20–H30···O3	1.081	2.405[a]	2.720	94.8	0.013	
C15–H28···O1	1.077	2.185[a]	2.888	120.1	0.013	
C21–H31···O2	1.081	2.433	3.364	127.6	0.012	
C22–H32···O5	1.083	2.435[a]	2.748	94.7	0.011	

[a]Intramolecular.

in CRYSTAL17 (Dovesi et al., 2018). The basis sets for the H, C, N, and O atoms in the calculation were those of Gatti et al. (1994). The calculations were run on a 3.5 GHz PC using 8 *k*-points and the B3LYP functional and took ∼79 h.

III. RESULTS AND DISCUSSION

The root-mean-square Cartesian displacements between the Rietveld-refined and DFT-optimized structures of nicarbazin are 0.069 Å for DNC and 0.026 Å for HDP (Figures 3 and 4). The excellent agreement provides strong evidence that the structure is correct (van de Streek and Neumann, 2014). The following discussion concentrates on the DFT-optimized structure. The asymmetric unit (with atom numbering) is illustrated in Figure 5. The best view of the crystal structure is down the *b*-axis (Figure 6). Prominent is the parallel stacking of both DNC and HDP molecules. The mean plane of the DNC molecule is 18,1,−5, and that of the HDP molecule is 6,−3,16. The Mercury Aromatic Analyser indicates two strong interactions between the DNC molecules, with distances of 4.19 Å. Strong hydrogen bonds link the molecules into layers parallel to the *ab*-plane

All of the bond distances, bond angles, and torsion angles fall within the normal ranges indicated by a Mercury Mogul Geometry check (Macrae et al., 2020). Quantum chemical geometry optimization of isolated DNC and HDP molecules

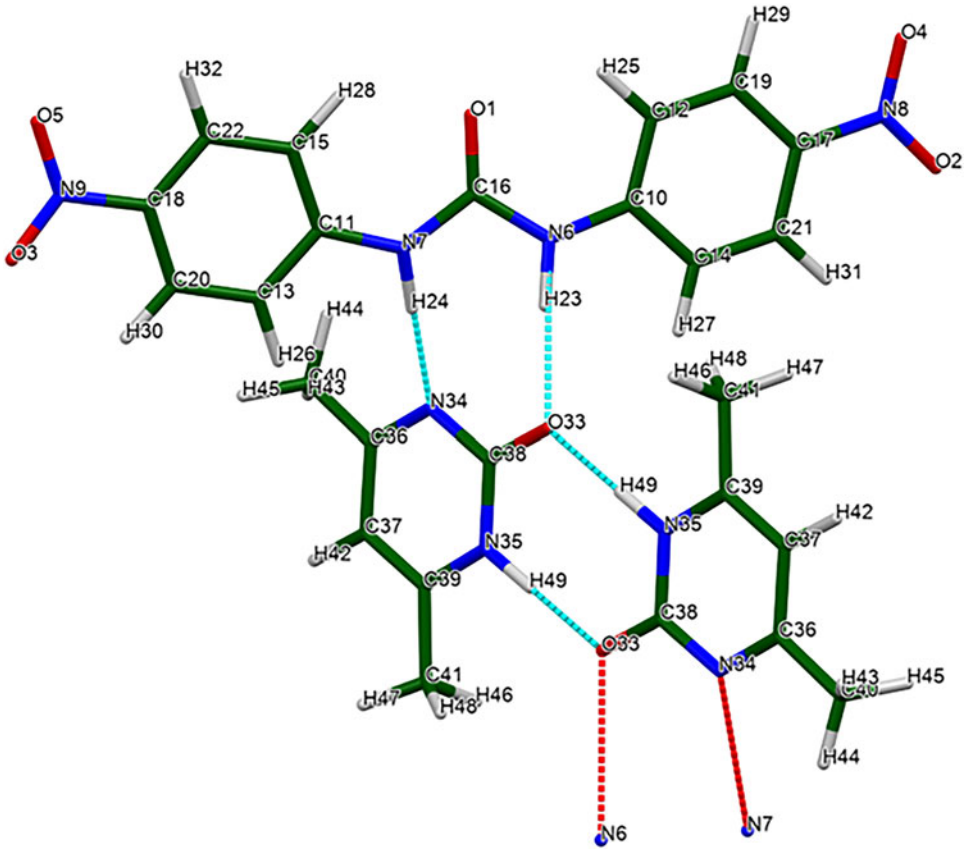

Figure 7. The principal hydrogen bonds in the crystal structure of nicarbazin. Image generated using Mercury (Macrae et al., 2020).

https://doi.org/10.1017/S0885715624000125 Published online by Cambridge University Press

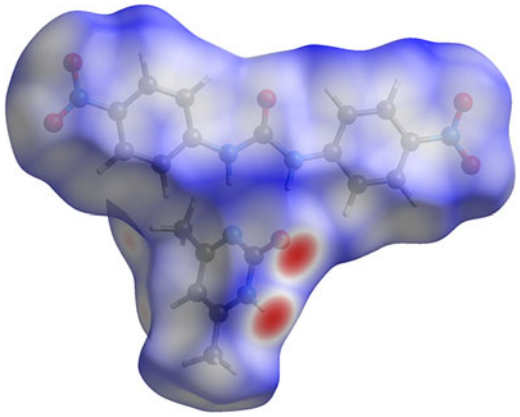

Figure 8. The Hirshfeld surface of nicarbazin. Intermolecular contacts longer than the sums of the van der Waals radii are colored blue, and contacts shorter than the sums of the radii are colored red. Contacts equal to the sums of radii are white. Image generated using CrystalExplorer17 (Turner et al., 2017).

(DFT/B3LYP/6-31G*/water) using Spartan '18 (Wavefunction, 2020) indicated that both molecules are in essentially their minimum-energy conformations. Solid-state interactions, though important to the crystal energy, do not result in molecular changes.

Analysis of the contributions to the total crystal energy of the structure using the Forcite module of Materials Studio (Dassault Systèmes, 2021) suggests that the intramolecular deformation energy contributions are small and equally distributed among bond, angles, and torsion terms. The intermolecular energy is dominated by electrostatic attractions, which in this force field analysis also include hydrogen bonds. The hydrogen bonds are better analyzed using the results of the DFT calculation.

Hydrogen bonds are prominent in the structure (Table I). The DNC and HDP molecules are linked by two strong N–H···O and N–H···N hydrogen bonds, and the HDP molecules are linked into centrosymmetric dimers by another N–H···O hydrogen bond (Figure 7). Both the HDP···HDP and DNC···HDP links have graph sets *R2,2(8)* (Etter, 1990; Bernstein et al., 1995; Shields et al., 2000). These strong hydrogen bonds link the molecules into layers parallel to the *ab*-plane. The energies of the N–H···O hydrogen bonds were calculated using the correlation of Wheatley and Kaduk (2019). Both methyl and ring hydrogen atoms in the HDP act as donors in intermolecular C–H···O hydrogen bonds. Most of the ring hydrogen atoms in the DNC participate in intramolecular C–H···O hydrogen bonds to the nitro groups and the urea carbonyl oxygen atom O1.

The volume enclosed by the Hirshfeld surface of nicarbazin (Figure 8, Hirshfeld, 1977; Turner et al., 2017) is 483.11 Å^3, 98.35% of 1/2 the unit cell volume. The packing density is thus fairly typical. The only significant close contacts (red in Figure 8) involve the hydrogen bonds. The volume/non-hydrogen atom is smaller than usual, at 15.8 Å^3.

The Bravais–Friedel–Donnay–Harker (Bravais, 1866; Friedel, 1907; Donnay and Harker, 1937) morphology suggests that we might expect platy morphology for nicarbazin, with {001} as the major faces, or elongated morphology with [100] as the long axis. A second-order spherical harmonic model was included in the refinement. The texture index was 1.001(0), indicating that the preferred orientation was slight in this rotated capillary specimen.

IV. DEPOSITED DATA

The Crystallographic Information Framework (CIF) files containing the results of the Rietveld refinement (including the raw data) and the DFT geometry optimization were deposited with the ICDD. The data can be requested at pdj@icdd.com.

ACKNOWLEDGEMENTS

Use of the Advanced Photon Source at Argonne National Laboratory was supported by the U. S. Department of Energy, Office of Science, Office of Basic Energy Sciences, under Contract No. DE-AC02-06CH11357. This work was partially supported by the International Centre for Diffraction Data. We thank Lynn Ribaud and Saul Lapidus for their assistance in the data collection.

CONFLICTS OF INTEREST

The authors have no conflicts of interest to declare.

REFERENCES

Antao, S. M., I. Hassan, J. Wang, P. L. Lee, and B. H. Toby. 2008. "State-of-the-Art High-Resolution Powder X-Ray Diffraction (HRPXRD) Illustrated with Rietveld Refinement of Quartz, Sodalite, Tremolite, and Meionite." *Canadian Mineralogist* 46: 1501–9.

Bernstein, J., R. E. Davis, L. Shimoni, and N. L. Chang. 1995. "Patterns in Hydrogen Bonding: Functionality and Graph Set Analysis in Crystals." *Angewandte Chemie International Edition in English* 34: 1555–73.

Bravais, A. 1866. *Etudes Cristallographiques*. Paris, Gauthier Villars.

Bruno, I. J., J. C. Cole, M. Kessler, J. Luo, W. D. S. Motherwell, L. H. Purkis, B. R. Smith, R. Taylor, R. I. Cooper, S. E. Harris, and A. G. Orpen. 2004. "Retrieval of Crystallographically-Derived Molecular Geometry Information." *Journal of Chemical Information and Computer Sciences* 44: 2133–44.

Crystal Impact - Dr. H. Putz & Dr. K. Brandenburg. 2022. *Diamond - Crystal and Molecular Structure Visualization*. Kreuzherrenstr. 102, 53227 Bonn, Germany. https://www.crystalimpact.de/diamond.

Dassault Systèmes. 2021. *Materials Studio 2021*. San Diego, CA, BIOVIA.

Donnay, J. D. H., and D. Harker. 1937. "A New Law of Crystal Morphology Extending the Law of Bravais." *American Mineralogist* 22: 446–6.

Dovesi, R., A. Erba, R. Orlando, C. M. Zicovich-Wilson, B. Civalleri, L. Maschio, M. Rerat, S. Casassa, B. Baima, J. Salustro, and B. Kirtman. 2018. "Quantum-Mechanical Condensed Matter Simulations with CRYSTAL." *WIREs Computational Molecular Science* 8: e1360.

Etter, M. C. 1990. "Encoding and Decoding Hydrogen-Bond Patterns of Organic Compounds." *Accounts of Chemical Research* 23: 120–6.

Favre-Nicolin, V., and R. Černý. 2002. "FOX, Free Objects for Crystallography: A Modular Approach to Ab Initio Structure Determination from Powder Diffraction." *Journal of Applied Crystallography* 35: 734–43.

Friedel, G. 1907. "Etudes sur la loi de Bravais." *Bulletin de la Société Française de Minéralogie* 30: 326–455.

Gates-Rector, S., and T. Blanton. 2019. "The Powder Diffraction File: A Quality Materials Characterization Database." *Powder Diffraction* 39: 352–60.

Gatti, C., V. R. Saunders, and C. Roetti. 1994. "Crystal-Field Effects on the Topological Properties of the Electron-Density in Molecular Crystals - The Case of Urea." *Journal of Chemical Physics* 101: 10686–96.

https://doi.org/10.1017/S0885715624000125 Published online by Cambridge University Press

Groom, C. R., I. J. Bruno, M. P. Lightfoot, and S. C. Ward. 2016. "The Cambridge Structural Database." *Acta Crystallographica Section B: Structural Science, Crystal Engineering and Materials* 72: 171–9.

Hirshfeld, F. L. 1977. "Bonded-Atom Fragments for Describing Molecular Charge Densities." *Theoretica Chemica Acta* 44: 129–38.

Kaduk, J. A., C. E. Crowder, K. Zhong, T. G. Fawcett, and M. R. Suchomel. 2014. "Crystal Structure of Atomoxetine Hydrochloride (Strattera), $C_{17}H_{22}NOCl$." *Powder Diffraction* 29: 269–73.

Kim, S., J. Chen, T. Cheng, A. Gindulyte, J. He, S. He, Q. Li, B. A. Shoemaker, P. A. Thiessen, B. Yu, L. Zaslavsky, J. Zhang, and E. E. Bolton. 2019. "Pubchem 2019 Update: Improved Access to Chemical Data." *Nucleic Acids Research* 47: D1102–9. doi:10.1093/nar/gky1033.

Lee, P. L., D. Shu, M. Ramanathan, C. Preissner, J. Wang, M. A. Beno, R. B. Von Dreele, L. Ribaud, C. Kurtz, S. M. Antao, X. Jiao, and B. H. Toby. 2008. "A Twelve-Analyzer Detector System for High-Resolution Powder Diffraction." *Journal of Synchrotron Radiation* 15: 427–32.

Macrae, C. F., I. Sovago, S. J. Cottrell, P. T. A. Galek, P. McCabe, E. Pidcock, M. Platings, G. P. Shields, J. S. Stevens, M. Towler, and P. A. Wood. 2020. "*Mercury 4.0*: From Visualization to Design and Prediction." *Journal of Applied Crystallography* 53: 226–35.

MDI. 2022. *JADE Pro Version 8.6 (Computer Software)*. Livermore, CA, USA, Materials Data.

O'Boyle, N., M. Banck, C. A. James, C. Morley, T. Vandermeersch, and G. R. Hutchison. 2011. "Open Babel: An Open Chemical Toolbox." *Journal of Chemical Informatics* 3: 33. doi:10.1186/1758-2946-3-33.

Rogers, E. F., R. D. Brown, J. E. Brown, D. M. Kazazis, W. J. Leanza, J. R. Nichols, D. A. Ostlind, and T. M. Rodino. 1983. "Nicarbazin Complex Yields Dinitrocarbanilide as Ultrafine Crystals with Improved Anticoccidial Activity." *Science* 222: 630–2.

Shields, G. P., P. R. Raithby, F. H. Allen, and W. S. Motherwell. 2000. "The Assignment and Validation of Metal Oxidation States in the Cambridge Structural Database." *Acta Crystallographica Section B: Structural Science* 56: 455–65.

Sykes, R. A., P. McCabe, F. H. Allen, G. M. Battle, I. J. Bruno, and P. A. Wood. 2011. "New Software for Statistical Analysis of Cambridge Structural Database Data." *Journal of Applied Crystallography* 44: 882–6.

Toby, B. H., and R. B. Von Dreele. 2013. "GSAS II: The Genesis of a Modern Open Source All Purpose Crystallography Software Package." *Journal of Applied Crystallography* 46: 544–9.

Turner, M. J., J. J. McKinnon, S. K. Wolff, D. J. Grimwood, P. R. Spackman, D. Jayatilaka, and M. A. Spackman. 2017. *CrystalExplorer17*. (University of Western Australia). https://crystalexplorer.scb.uwa.edu.au.

van de Streek, J., and M. A. Neumann. 2014. "Validation of Molecular Crystal Structures from Powder Diffraction Data with Dispersion-Corrected Density Functional Theory (DFT-D)." *Acta Crystallographica Section B: Structural Science, Crystal Engineering and Materials* 70: 1020–32.

Wang, J., B. H. Toby, P. L. Lee, L. Ribaud, S. M. Antao, C. Kurtz, M. Ramanathan, R. B. Von Dreele, and M. A. Beno. 2008. "A Dedicated Powder Diffraction Beamline at the Advanced Photon Source: Commissioning and Early Operational Results." *Revue of Scientific Instruments* 79: 085105.

Wavefunction, Inc. 2020. Spartan '18 Version 1.4.5, Wavefunction Inc., 18401 Von Karman Ave., Suite 370, Irvine CA 92612.

Wheatley, A. M., and J. A. Kaduk. 2019. "Crystal Structures of Ammonium Citrates." *Powder Diffraction* 34: 35–43.

https://doi.org/10.1017/S0885715624000125 Published online by Cambridge University Press